Wireless Powered Intelligent Radio Environment with Non-Linear Energy Harvesting

Zheng Chu, *Member, IEEE*, Pei Xiao, *Senior Member, IEEE*, De Mi, *Member, IEEE*, Wanming Hao, *Member, IEEE*, Zihuai Lin *Senior Member, IEEE*, Qingchun Chen, *Senior Member, IEEE*, and Rahim Tafazolli, *Senior Member, IEEE*

***Abstract*—This paper investigates a wireless powered intelligent radio environment, where a fractional non-linear energy harvesting (NLEH) is proposed to enable an intelligent reflecting surface (IRS) assisted wireless powered Internet of Things (WP IoT) network. The IRS engages in downlink wireless energy transfer (WET) and uplink wireless information transfer (WIT). We aim to improve the overall performance of the considered network, and the approach is to maximize its sum throughput subject to constraints of two different types of IRS beam patterns and time durations. To solve the formulated problem, we first consider the Lagrange dual method and Karush-Kuhn-Tucker (KKT) conditions to optimally design the time durations in closed-form. Then, a quadratic transformation (QT) is proposed to iteratively transform the fractional NLEH model into the subtractive form, where the IRS phase shifts are optimally derived by the Complex Circle Manifold (CCM) method in each iteration. Finally, numerical results are demonstrated to promote the proposed scheme in comparison to the benchmark schemes, where the benefits are induced by the IRS compared with the benchmark schemes.**

***Index Terms*—Intelligent radio environment, intelligent reflecting surface (IRS), non-linear energy harvesting (NLEH), phase shifts, Quadratic Transformation (QT), Complex Circle Manifold (CCM)**

I. INTRODUCTION

Intelligent radio environment has been regarded as one of promising and revolutionized paradigms in beyond fifth-generation (B5G) or sixth-generation (6G) networks. Its main purpose is to introduce a holographic communication model by adjusting wireless propagations so as to improve the network throughput and energy efficiency by introducing a novel passively reflecting communication mode, namely, *intelligent reflecting surface* (IRS) [1], [2]. An IRS is made up of plentiful low-cost and small-size reflecting arrays/elements, each of which aims to induce a certain phase shift to perform the passive reception and reflection on the intended signals [3], [4]. Hence, the IRS is a better fit to improve spectral efficiency or system throughput for existing wireless networks without the redesign of the network architectures and the extra energy consumption.

This work was supported in part by the Engineering and Physical Sciences Research Council (EPSRC) Project under Grant EP/P03456X/1. The work of W. Hao was supported in part by the National Natural Science Foundation of China under Grant 62101499.

Z. Chu, P. Xiao, D. Mi, and R. Tafazolli are with 5GIC & 6GIC, Institute for Communication Systems (ICS), University of Surrey, Guildford GU2 7XH, UK. (Email: andrew.chuzheng7@gmail.com; p.xiao@surrey.ac.uk; d.mi@surrey.ac.uk; r.tafazolli@surrey.ac.uk)

W. Hao is with the School of Information Engineering, Zhengzhou University, Zhengzhou 450001, China. (Email: wmhao@hotmail.com).

Zihuai Lin is with the School of Electrical and Information Engineering, University of Sydney, Sydney, NSW 2006, Australia. (Email: zihuai.lin@sydney.edu.au)

Qingchun Chen is with with the Research Center of Intelligent Communication Engineering, Huangpu Research and Graduate School, Guangzhou University, Guangzhou 510006, China, and also with the Department of Electronics and Communication Engineering, School of Electronics and Communication Engineering, Guangzhou University, Guangzhou 510006, China. (Email: qcchen@gzhu.edu.cn).

In recent years, Internet of Things (IoT) has been exploited to connect myriads of wireless devices (WDs), i.e., sensors and machines, with the majority of them featuring small-size and low-power, as well as being typically vulnerable to the energy-constrained issue. Existing research endeavours focus on the periodical maintenance or regular replacement for the IoT sensors batteries in order to extend their operational lifetime, as well as the design of the optimal energy-efficient policy for IoT networks. These solutions may incur various challenges or even are not able to enjoy energy-efficient benefits. For instance, most of IoT sensors are employed for remote monitoring for emergence services, which are generally deployed in some challenging environments leading to difficulty for the maintenance of the sensors' batteries. In addition, the energy-efficient optimization policies may introduce a very high computational complexity, making it more difficult to configure the hardware architecture of IoT sensors. Thus, the energy-limited battery lifetime of IoT sensors still remains unconquered [5].

In order to conquer the energy-constrained issue for the battery of IoT sensors, radio frequency wireless energy transfer (RF WET) has recently been emerged to exploit the electromagnetic wave (EW). Specifically, multiple WDs collect energy from RF signal radiated from a dedicated energy supply in wireless fashion, and the harvested energy is utilized for future wireless information transfer (WIT). This procedure facilitates a *well-known* name, i.e., wireless powered communication network (WPCN), where a classic "*harvest-then-transmit*" was adopted to coordinate the transmission time duration for the WET and WIT [5]. By provisioning with stable and controllable energy supplies, the WPCN is able to effectively enhance energy-efficient performance of IoT sensors to refurbish their own battery instead of the traditional maintenance or replacement. Hence, the WPCN confirms its energy-efficient highlights, which is a better fit to apply this promising technique in IoT networks.

A. Literature Review

Recently, various existing works investigated the integration of IRS and wireless powered communications (WPC), which aims to simultaneously improve energy collection and information delivery capabilities by passively controlling energy/information reflection [6]–[13]. In [6], the integration of IRS and simultaneous wireless information and power transfer (SWIPT) was considered in a multiple-input multiple-output (MISO) downlink system. Specifically, the weighted sum harvested power (WSHP) is maximized to jointly design the transmit precoders for information transmission and energy collection, as well as the passive reflection coefficients at the IRS. Also, the Rate-Energy (R-E) trade-off was exploited to achieve the high passive beamforming gain and the WET efficiency enhancement. This scenario has been extended to a distributed IRSs case in [7], specifically, a penalty-based approach was proposed to iteratively solve the transmit power minimization (TPM) problem to confirm its benefits induced by IRS for WET coverage and significant power saving performance gain. In [8], the weighted sum rate (WSR) is maximized in a MIMO SWIPT system subject to the constraints of transmit power budget and energy harvesting requirement. By exploiting the iterative block coordinate descent (IBCD) algorithm, the formulated problem was decomposed into several sub-problems, which are separately solved to jointly design the transmit precoders and the passive IRS phase shifts.

The IRS was introduced in the WPCN to engage energy and information reflections in [9], where multiple IoT devices first harvest energy from RF signal actively radiated from a power station (PS) as well as passively reflected from the IRS. Then, each IoT device uses the collected energy to deliver its own message to an access point (AP) with the aid of IRS by using time-division multiple access (TDMA). The IRS beam patterns and the time slots are jointly designed to maximize the sum throughput at the downlink WET and uplink WIT. The dual method and KKT conditions were employed to derive the transmission time scheduling, and the Majorization-Minimization (MM) algorithm was utilized to optimally derive the closed-form IRS phase shifts. Moreover, the time switching and power splitting protocols were applied in the IRS to schedule a part of RF energy to guarantee its control circuit operation [10], [11]. Specifically, the semidefinite programming (SDP) relaxation and one-dimensional numerical method were considered to determine the optimal transmission time scheduling and IRS phase shifts [10], while [11] proposed a novel low complexity scheme based on the Lagrange dual method, KKT conditions, and MM algorithm to optimally design the closed-form transmission time scheduling and IRS phase shifts. In [12], non-orthogonal multiple access (NOMA) scheme was introduced in an IRS assisted WPCN. Specifically, a hybrid AP (HAP) first broadcasts energy to multiple IoT devices, which then deliver their own information using NOMA. By maximizing the sum throughput, different IRS passive beam patterns of downlink WET and uplink WIT were proved to be identical, which can mitigate the extra signalling overhead and computational complexity. Also, the semi-closed-form IRS phase shifts can be derived by using an alternating optimization (AO) algorithm. Similar scenario was extended to multi-cluster case, where multiple IoT devices were grouped into clusters [13]. The IRS participates to passively reflect energy and information at the downlink WET and uplink WIT durations, respectively. The hybrid TDMA and NOMA protocol were considered to balance complexity and performance during the WIT phase, where each cluster transmits information by TDMA and each IoT device share one sub-time slot by NOMA to deliver information [13].

Although the aforementioned works focused on the application of the IRS to enhance WET and WIT by jointly optimizing different types of IRS's phase shifts, these references only considered the linear energy harvesting (LEH) model at the IoT devices, which assumes the constant energy conversion efficiency. Specifically, the the harvested energy in the LEH model generally considers an ideally linear function with respect to the RF received power, which fails to capture the saturation state in large input power level. Hence, a more practical non-linear EH (NLEH) model is a better fit to capture this saturation property. Recently, a few existing works investigated the NLEH model in the integration of the IRS and WPC [14]–[16]. The sigmoid function based NLEH model was studied to exploit the minimization of the transmit power [14] and the maximization of the minimum energy efficiency [15], which alternately optimizes energy and information beamformers, as well as the IRS beam pattern. Also, another error function based NLEH model has been applied in the IRS assisted SWIPT system [16], where robust active transmit beamforming, IRS passive beam pattern, and the users' PS factor were designed by the IBCD algorithm. Very recently, the NLEH model was integrated into the IRS assisted WPCN in [17], specifically, the RF energy radiated from the HAP was minimized to jointly design the HAP energy and receiving information beamforming vectors, the power allocation of the users, as well as the IRS phase shifts. The AO and difference-of-convex (DC) programming were applied to address this formulated problem. Although these references characterized the NLEH models in different IRS assisted WPC systems, these NLEH models could bring a more complicated harvested power/energy, which further leads to a more complicated problem formulation such that the IRS phase shifts can only be numerically optimized, e.g., the SDP relaxation. This may result in a loose relaxation so as to incur a higher rank for the SDP relaxed solution, which may require the Gaussian randomization to obtain a feasible solution of the IRS phase shifts, thus leading to a high computational complexity of the IRS phase shift optimization due to the interior-point methods [10].

Inspired by this research background, this paper exploits a novel fractional NLEH model in a wireless powered intelligent radio environment. In the following, we summarize the main contributions of this paper.

1) First, we investigate a wireless powered intelligent radio environment, where an IRS operates in the passive reflection mode to improve downlink WET and uplink WIT capabilities. Also, we propose to apply a novel NLEH model based on the fraction function to characterize the non-linearity and saturation of practical energy

harvester. According to the best of the authors' knowledge, there is no published work that investigated this fractional NLEH model in wireless powered intelligent radio environment.

2) To capture the overall performance of the system model under consideration, the sum throughput is maximized subject to the constraints of the transmission time scheduling, and the IRS phase shifts of the downlink WET and uplink WIT durations. These coupled variables can lead to the non-convexity of the formulated problem, which in turn makes it intractable.

3) In order to deal with this non-convex issue, we propose to use the Lagrange dual methods and KKT conditions to derive the transmission time scheduling of the downlink WET and upplink WIT in a closed form. Next, the IRS phase shifts can be separately derived at each uplink WIT duration by the triangle inequality. To derive the IRS phase shifts of the downlink WET, a quadratic transformation (QT) is proposed to iteratively transform the fractional NLEH model into the subtractive form for the tractability, and the locally optimal IRS phase shifts of the downlink WET are designed by employing the complex circle manifold (CCM) method at each iteration.

4) Finally, numerical results are demonstrated to validate the convergence of the proposed algorithm, and the effectiveness of the proposed NLEH model, which highlights the optimality of the IRS phase shifts, and the benefits induced by the IRS in comparison to the benchmark schemes.

The remainder of this paper is summarized as follows. Section II illustrates the system model. Section III exhibits the potentials of the fractional NLEH model on the wireless powered intelligent radio environment. Numerical results are presented in Section IV to highlight the proposed scheme. Finally, this paper is concluded in Section V.

II. System Model

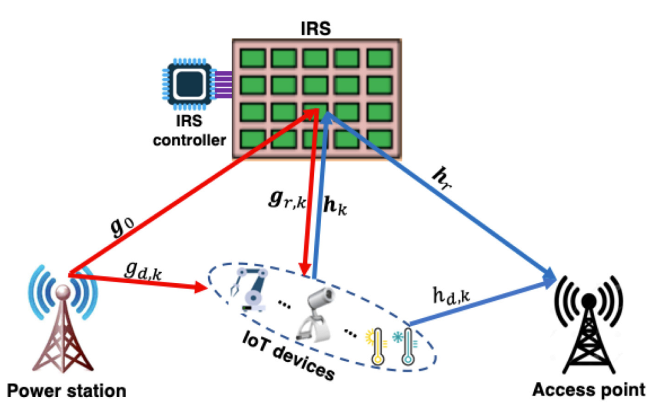

Fig. 1: An IRS assisted wireless powered IoT network.

This section presents a wireless powered intelligent radio environment, in which an IRS aims to engage the passive reflection of energy and information signals. The considered system is made up with two phases: downlink WET and uplink WIT. During downlink WET, multiple IoT devices (i.e., denoted by $\mathcal{U}_k,\ \forall k \in [1, K]$) collect energy wirelessly radiated from a PS, each of which then utilizes collected energy to deliver its individual message to an AP during uplink WIT. Assume that the IRS is composed of N reflecting elements, whereas the others have a single antenna each. Generally, it is assumed that the IRS assisted wireless powered IoT network considers the time-division multiplexing operation via the generic "harvest-then-transmit/reflection" protocol [9], [11]. Without loss of generality, we assume that each channel coherence block consists of multiple time frames and the operation time of each frame is denoted by T. Let us denote τ_0 as the time duration of downlink WET, while the time duration of $\mathcal{U}_k,\ \forall k \in [1, K]$ is denoted by τ_k at the uplink WIT, and $\sum_{k=0}^{K} \tau_k = T$. Although the downlink WET and uplink WIT time slots of each IoT device are independent of each other, it is assumed that each device is equipped with a rechargeable battery so as to store the harvested energy during the downlink WET to support its uplink WIT. In addition, the IRS generates two types of passive beamforming patterns to engage energy and information reflections at downlink WET and uplink WIT, respectively. Specifically, we set the passive beamforming as the diagonal matrix $\mathbf{\Theta}_k = \text{diag}\left[\beta_{k,1}\exp(j\alpha_{k,1}), ..., \beta_{k,N}\exp(j\alpha_{k,N})\right],\ \forall k \in [0, K],\ \forall n \in [1, N]$, where $k = 0$ and $k = 1, ..., K$ denote the respective IRS beam patterns of downlink WET and uplink WIT. Each element of $\mathbf{\Theta}_k$ represents the refection coefficient, where $\beta_{k,n}$ and $\alpha_{k,n}$ denote its amplitude and phase shift, respectively. Note that $\mathbf{\Theta}_k = \mathbf{\Theta}_{\beta,k}\mathbf{\Theta}_{\alpha,k},\ \forall k \in [0, K]$, where $\mathbf{\Theta}_{\beta,k} = \text{diag}\left[\beta_{k,1}, ..., \beta_{k,N}\right]$, and $\mathbf{\Theta}_{\alpha,k} = \text{diag}\left[\exp(j\alpha_{k,1}), ..., \exp(j\alpha_{k,N})\right]$. Moreover, let us denote $g_{d,k} \in \mathbb{C}^{1\times 1}$, $h_{d,k} \in \mathbb{C}^{1\times 1}$, $\mathbf{g}_0 \in \mathbb{C}^{1\times N}$, $\mathbf{g}_{r,k} \in \mathbb{C}^{N\times 1}$, $\mathbf{h}_k \in \mathbb{C}^{1\times N}$, and $\mathbf{h}_r \in \mathbb{C}^{N\times 1}$, as the channel coefficients of the PS-$\mathcal{U}_k$, the $\mathcal{U}_k$-AP, the PS-IRS, the IRS-$\mathcal{U}_k$, the $\mathcal{U}_k$-IRS, the IRS-AP links, respectively. In the duration of WET τ_0, we first express the harvested energy at $\mathcal{U}_k,\ \forall k \in [1, K]$ as [9]

$$E_{\text{LEH},k} = \eta\tau_0 P_0 \left|\mathbf{g}_0\mathbf{\Theta}_{\beta,0}\mathbf{\Theta}_{\alpha,0}\mathbf{g}_{r,k} + g_{d,k}\right|^2, \tag{1}$$

where P_0 denotes the transmit power of the PS, and η denotes the energy conversion efficiency. Equation (1) is known as the LEH model, and its energy conversion efficiency η is typically set to be a constant and is adopted to approximate a linear region of a practical non-linear harvester. However, the energy harvesting circuits practically result in a non-linear conversion model, where the output power is typically a non-linear function in terms of the RF input power [10]. This is originated from the fact that the harvested power first linearly increases with respect to the received power and then gradually becomes saturated with a high received power threshold. In order to exploit the approximated non-linear EH (NLEH) properties and the saturation region of a practical energy harvester, this paper proposes a fractional NLEH model, where the harvested energy at $\mathcal{U}_k$ is written as

$$E_{\text{NLEH},k} = \tau_0 \frac{(a_k c_k - b_k) P_0 \left|\mathbf{g}_0\mathbf{\Theta}_{\beta,0}\mathbf{\Theta}_{\alpha,0}\mathbf{g}_{r,k} + g_{d,k}\right|^2}{c_k P_0 \left|\mathbf{g}_0\mathbf{\Theta}_{\beta,0}\mathbf{\Theta}_{\alpha,0}\mathbf{g}_{r,k} + g_{d,k}\right|^2 + c_k^2}, \tag{2}$$

where $a_k = 2.463$, $b_k = 1.635$, and $c_k = 0.826$ denote the positive constants determined in [18].[1] The fractional NLEH

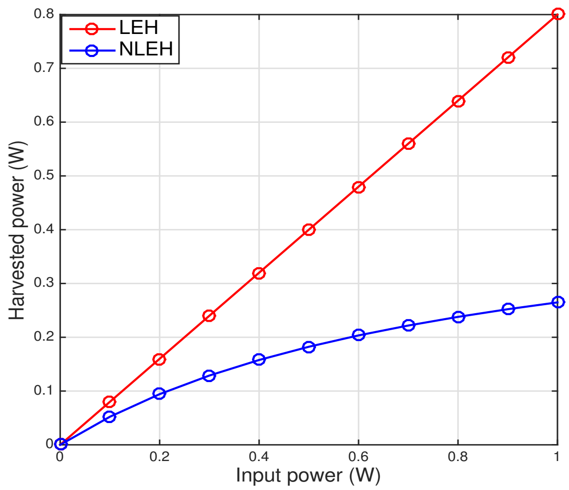

Fig. 2: Comparison between NLEH and LEH models.

model this paper employs has been experimentally validated by the measurement data [18, Fig. 1], where it captures the characteristics of the energy harvester, i.e., non-linear distortion or saturation. In addition, in a practical system, such as the wireless energy harvesting relaying or WET application, each IoT device typically features low-power consumption, and is vulnerable to energy-limited issue. As such, it requires the harvest energy to support the information forwarding or delivery. The existing LEH model typically employs a constant energy conversion efficiency η to characterize the energy harvester of the device. Whereas the NLEH model considers the fractional programming to examine the practical energy harvester such that the harvested power can be considered as a fractional function of the received RF power, instead of using the conversion efficiency η in the LEH model. Each IoT device employs this fractional model to mathematically capture the harvested power behaviour to guarantee that it does not exceed its rechargeable battery capacity. In Fig. 2, we provide a comparison between NLEH and LEH models in terms of harvested power, where it can be seen that the LEH model significantly outperforms the NLEH model, and the gap between them becomes larger with the input power.

[1]Our considered NLEH model in (2) is different from that in [10], which considered a straightforward two-piece linear EH model and is made up of a LEH model and a saturated power threshold. The proposed NLEH model in (2) integrally considers these two portions by using a fractional model. In addition, the authors of [18] employed curve fitting to obtain the fractional NLEH from the measurement data, where our paper adopts the same NLEH parameter setup. However, [18] only focused on a wireless energy harvesting system to formulate the harvested power model, and the performance analysis was derived to validate the considered NLEH model for different fading channel configurations. This model has not yet been investigated in the IRS-assisted wireless powered IoT networks in the existing literature. This makes our system model more complicated than [18], where the received RF power at each IoT device is from two paths, i.e., direct PS-device link and cascaded PS-IRS-device link. This further complicates problem formulation in this paper, which consists of the multiple coupled variables, i.e., two passive beam patterns and transmission time scheduling of the downlink WET and uplink WIT, which cannot be easily solved by the existing methods [9]–[11].

This is originated from the fact that the energy conversion efficiency η of the LEH model in (1) is ideal, providing an upper bound on that of the NLEH model in (2). Then, each IoT device uses the harvested energy within downlink WET duration to deliver its individual information to the AP within uplink WIT duration of τ_k, $\forall k \in [1, K]$. Thus, the achievable throughput of $\mathcal{U}_k$ at the AP is given by

$$R_k = \tau_k \log\left(1 + \frac{t\tau_0(a_k c_k - b_k)t_{0,k}t_{1,k}}{\tau_k\left(c_k P_0 t_{0,k} + c_k^2\right)}\right), \tag{3}$$

where $t = \frac{P_0}{\sigma^2}$, $t_{0,k} = |\mathbf{g}_0 \mathbf{\Theta}_{\beta,0}\mathbf{\Theta}_{\alpha,0}\mathbf{g}_{r,k} + g_{d,k}|^2$, and $t_{1,k} = |\mathbf{h}_k \mathbf{\Theta}_{\beta,k}\mathbf{\Theta}_{\alpha,k}\mathbf{h}_r + h_{d,k}|^2$.

III. Sum Throughput Maximization of IRS Assisted WP IoT Network with NLEH Model

This section aims at a maximization problem of the system sum throughput, subject to the constraints of two different types of IRS beam patterns and the transmission time durations of the downlink WET and uplink WIT. As such, this formulated problem is given by

$$\max_{\mathbf{\Theta}_\alpha, \boldsymbol{\tau}} \sum_{k=1}^{K} R_k, \tag{4a}$$

$$s.t.\ \mathbf{\Theta}_\alpha = \{\mathbf{\Theta}_{\alpha,k}\}_{k=0}^{K}, \ |\exp(j\alpha_{k,n})| = 1, \quad \forall k \in [0, K],\ \forall n \in [1, N], \tag{4b}$$

$$\boldsymbol{\tau} = \{\tau_k\}_{k=0}^{K}, \ \sum_{k=0}^{K} \tau_k \le T,\ \boldsymbol{\tau} \succeq \mathbf{0}. \tag{4c}$$

In problem (4), (4b) and (4c) are the unit-modulus IRS phase shift and transmission time scheduling constraints, respectively. These coupled variables, i.e., $\mathbf{\Theta}_\alpha$ and $\boldsymbol{\tau}$, lead to the non-convexity of problem (4), which is not able to be directly solved. To circumvent this issue, we first employ the dual method and the KKT conditions to optimally derive the time scheduling $\boldsymbol{\tau}$. Then, we propose the QT and CCM methods to iteratively design the optimal IRS phase shifts in closed-form. Now, let us consider the following mathematical transformations to tackle the IRS phase shifts for tractability,

$$t_{0,k} = |\mathbf{g}_0 \mathbf{\Theta}_{\beta,0}\mathbf{\Theta}_{\alpha,0}\mathbf{g}_{r,k} + g_{d,k}|^2 = |\boldsymbol{\theta}_{\alpha,0}\mathbf{a}_k + g_{d,k}|^2, \tag{5a}$$

$$t_{1,k} = |\mathbf{h}_k \mathbf{\Theta}_{\beta,k}\mathbf{\Theta}_{\alpha,k}\mathbf{h}_r + h_{d,k}|^2 = |\boldsymbol{\theta}_{\alpha,k}\mathbf{b}_k + h_{d,k}|^2, \tag{5b}$$

where $\mathbf{a}_k = \mathrm{diag}\left(\bar{\mathbf{g}}_0\right)\mathbf{g}_{r,k}$, $\mathbf{b}_k = \mathrm{diag}\left(\bar{\mathbf{h}}_k\right)\mathbf{h}_r$, $\bar{\mathbf{g}}_0 = \mathbf{g}_0\mathbf{\Theta}_{\beta,0}$, $\bar{\mathbf{h}}_k = \mathbf{h}_k\mathbf{\Theta}_{\beta,k}$, $\boldsymbol{\theta}_{\alpha,k} = [\theta_{k,1}, ..., \theta_{k,N}] = [\exp(j\alpha_{k,1}), ..., \exp(j\alpha_{k,N})]$. Accordingly, problem (4) is equivalently reformulated as

$$\max_{\boldsymbol{\theta}_\alpha, \boldsymbol{\tau}} \sum_{k=1}^{K} \tau_k \log\left(1 + \frac{t\tau_0(a_k c_k - b_k)t_{0,k}t_{1,k}}{\tau_k\left(c_k P_0 t_{0,k} + c_k^2\right)}\right),$$

$$s.t.\ \boldsymbol{\theta}_\alpha = \{\boldsymbol{\theta}_{\alpha,k}\}_{k=0}^{K}, \ |\exp(j\alpha_{k,n})| = 1, \quad \forall k \in [0, K],\ \forall n \in [1, N], \tag{6a}$$

$$(4c). \tag{6b}$$

A. Optimized Transmission Time Scheduling

To solve problem (6), let us denote $A_k = t(a_k c_k - b_k)$, $B_k = c_k P_0$, and write its Lagrange dual function as

$$\mathcal{L}(\boldsymbol{\tau}, \mu) = \sum_{k=1}^{K} \tau_k \log\left(1 + \frac{\tau_0 A_k t_{0,k} t_{1,k}}{\tau_k (B_k t_{0,k} + c_k^2)}\right) - \mu \left(\sum_{k=0}^{K} \tau_k - T\right), \quad (7)$$

where $\mu \geq 0$ is the dual variable with (4c). Accordingly, the associated dual problem can be written as

$$\min_{\boldsymbol{\tau} \in \mathcal{S}_{\boldsymbol{\tau}}} \mathcal{L}(\boldsymbol{\tau}, \mu), \quad (8)$$

where $\mathcal{S}_{\boldsymbol{\tau}}$ denotes the feasible set of the time durations $\boldsymbol{\tau}$ in constraint (4c). Note that (6) is a convex problem in terms of $\boldsymbol{\tau}$ for given $\boldsymbol{\theta}_\alpha$, guaranteeing Slater's condition due to $\boldsymbol{\tau} \in \mathcal{S}_{\boldsymbol{\tau}}$ and (4c) [19]. Thus, the strong duality holds that the optimal solution of $\boldsymbol{\tau}$ satisfies the KKT conditions by solving (6) [9], [11]. As such, we have

$$\mu^* \left(\sum_{k=1}^{K} \tau_k^* - T\right) = 0. \quad (9a)$$

$$\frac{\partial \mathcal{L}}{\partial \tau_k} = 0.\ \forall k \in [1, K]. \quad (9b)$$

According to (9a), we have $\mu^* > 0$ to guarantee the equality holds in constraint (4c), i.e., $\sum_{k=0}^{K} \tau_k^* = T$. Then, we expand (9b) as

$$\frac{\partial \mathcal{L}}{\partial \tau_k} = \log\left(1 + \frac{\tau_0 A_k t_{0,k} t_{1,k}}{\tau_k (B_k t_{0,k} + c_k^2)}\right) - \frac{\tau_0 A_k t_{0,k} t_{1,k}}{\tau_k (B_k t_{0,k} + c_k^2) + \tau_0 A_k t_{0,k} t_{1,k}} - \mu = 0. \quad (10)$$

One can observe that (10) is a kind of function, i.e., $f(x) = \log(1+x) - \frac{x}{1+x}$, where $x = \frac{\tau_0 A_k t_{0,k} t_{1,k}}{\tau_k (B_k t_{0,k} + c_k^2)}$. It is a monotonically increasing function in terms of x. Via (10), it guarantees the following K equations of (10),

$$\frac{\tau_0 A_1 t_{0,1} t_{1,1}}{\tau_1 (B_1 t_{0,1} + c_1^2)} = \frac{\tau_0 A_2 t_{0,2} t_{1,2}}{\tau_2 (B_2 t_{0,2} + c_2^2)} =, ..., = \frac{\tau_0 A_K t_{0,K} t_{1,K}}{\tau_K (B_K t_{0,K} + c_K^2)}. \quad (11)$$

By defining $\frac{\tau_0 A_k t_{0,k} t_{1,k}}{\tau_k (B_k t_{0,k} + c_k^2)} = \frac{1}{\rho}$, we get

$$\tau_k = \frac{\rho \tau_0 A_k t_{0,k} t_{1,k}}{B_k t_{0,k} + c_k^2}. \quad (12)$$

We substitute (12) into $\sum_{k=1}^{K} \tau_k = T - \tau_0$ to obtain,

$$\rho = \frac{T - \tau_0}{\sum_{k=1}^{K} \frac{\tau_0 A_k t_{0,k} t_{1,k}}{B_k t_{0,k} + c_k^2}}, \quad (13)$$

which is plugged back into (12), the optimal solution of τ_k is derived as

$$\tau_k^* = \frac{A_k t_{0,k} t_{1,k} (T - \tau_0)}{(B_k t_{0,k} + c_k^2) \sum_{k=1}^{K} \frac{A_k t_{0,k} t_{1,k}}{B_k t_{0,k} + c_k^2}}. \quad (14)$$

By plugging (14) into problem (6), we have

$$\max_{\boldsymbol{\theta}_\alpha, \tau_0} f_0(\boldsymbol{\theta}_\alpha, \tau_0) = (T - \tau_0) \log\left(1 + \frac{\tau_0 \sum_{k=1}^{K} \frac{A_k t_{0,k} t_{1,k}}{B_k t_{0,k} + c_k^2}}{T - \tau_0}\right) \quad (15a)$$

$$s.t.\ (6a), 0 \leq \tau_0 \leq T. \quad (15b)$$

Note that (15) is still intractable due to (15a) and (6a). To solve (15), we first derive the optimal transmission time scheduling τ_0 for given IRS phase shifts $\boldsymbol{\theta}_\alpha$. To proceed, we calculate the first-order derivative of (15a) with τ_0 and set it to zero, which is given by

$$\left(1 + \frac{\tau_0 \sum_{k=1}^{K} \frac{A_k t_{0,k} t_{1,k}}{B_k t_{0,k} + c_k^2}}{T - \tau_0}\right) \log\left(1 + \frac{\tau_0 \sum_{k=1}^{K} \frac{A_k t_{0,k} t_{1,k}}{B_k t_{0,k} + c_k^2}}{T - \tau_0}\right) = \frac{T \sum_{k=1}^{K} \frac{A_k t_{0,k} t_{1,k}}{B_k t_{0,k} + c_k^2}}{T - \tau_0}. \quad (16)$$

Let us define $z = 1 + \frac{\tau_0 \sum_{k=1}^{K} \frac{A_k t_{0,k} t_{1,k}}{B_k t_{0,k} + c_k^2}}{T - \tau_0}$, and apply a few of mathematical manipulations, the following equation holds,

$$z \log(z) - z = \sum_{k=1}^{K} \frac{A_k t_{0,k} t_{1,k}}{B_k t_{0,k} + c_k^2} - 1 \quad (17)$$

According to (17) and Lambert $\mathcal{W}$ function, the optimal solution of τ_0 is derived as

$$\tau_0^* = \frac{\left[\exp\left(\mathcal{W}\left(\frac{\sum_{k=1}^{K} \frac{A_k t_{0,k} t_{1,k}}{B_k t_{0,k} + c_k^2} - 1}{\exp(1)}\right) + 1\right) - 1\right] T}{\sum_{k=1}^{K} \frac{A_k t_{0,k} t_{1,k}}{B_k t_{0,k} + c_k^2} + \exp\left(\mathcal{W}\left(\frac{\sum_{k=1}^{K} \frac{A_k t_{0,k} t_{1,k}}{B_k t_{0,k} + c_k^2} - 1}{\exp(1)}\right) + 1\right) - 1}. \quad (18)$$

B. Optimal Design of $\boldsymbol{\theta}_{\alpha,k}$

In Section III-A, we optimized the transmission time scheduling for given IRS phase shifts. Now, we solve problem (15) with respect to the IRS phase shifts, i.e., $\boldsymbol{\theta}_\alpha$.One can readily verify that the maximization of f_0 in (15) is equivalent to

$$\max_{\boldsymbol{\theta}} \sum_{k=1}^{K} \frac{A_k |\boldsymbol{\theta}_{\alpha,0} \mathbf{a}_k + g_{d,k}|^2 |\boldsymbol{\theta}_{\alpha,k} \mathbf{b}_k + h_{d,k}|^2}{B_k |\boldsymbol{\theta}_{\alpha,0} \mathbf{a}_k + g_{d,k}|^2 + c_k^2},$$
$$s.t.\ |\boldsymbol{\theta}_{\alpha,k}(n)| = 1, \forall k \in [0, K],\ \forall n \in [1, N]. \quad (19)$$

Problem (19) is not convex due to the sum of multiple fractional functions and the unit-modulus constraint. To solve it, we first derive the optimal solution of $\boldsymbol{\theta}_{\alpha,k},\ \forall k \in [1, K]$ via the following *theorem*.

Theorem 1: The optimal solution of $\boldsymbol{\theta}_{\alpha,k},\ \forall k \in [1, K]$ can be derived as

$$\boldsymbol{\theta}_{\alpha,k}^* = [\exp(j\alpha_{k,1}^*), ..., \exp(j\alpha_{k,N}^*)],$$
$$\alpha_{k,n}^* = \arg(h_{d,k}) - \arg(\mathbf{b}_k[n]), \quad (20)$$

where $\mathbf{b}_k[n],\ \forall k \in [1, K],\ \forall n \in [1, N]$, is the n-th element of $\mathbf{b}_k$.

Proof: From the objective function in (19), we can readily verify that it is a monotonically increasing function with respect to the term $|\boldsymbol{\theta}_{\alpha,k}\mathbf{b}_k + h_{d,k}|^2$, which follows that the maximization of problem (19) is equivalent to maximizing the term $|\boldsymbol{\theta}_{\alpha,k}\mathbf{b}_k + h_{d,k}|^2$ with the unit-modulus constraint $|\boldsymbol{\theta}_{\alpha,k}(n)| = 1,\ \forall k \in [1, K],\ \forall n \in [1, N]$. As such, the optimal solution of $\boldsymbol{\theta}_{\alpha,k}$ can be obtained by solving the following problem,

$$\begin{aligned} &\max_{\boldsymbol{\theta}_{\alpha,k}} \ |\boldsymbol{\theta}_{\alpha,k}\mathbf{b}_k + h_{d,k}|^2, \\ &\ s.t. \ |\boldsymbol{\theta}_{\alpha,k}(n)| = 1,\ \forall k \in [1, K],\ \forall n \in [1, N]. \end{aligned} \tag{21}$$

To proceed, we apply the triangle inequality to obtain the upper bound of the objective function in (21), which is given as

$$\begin{aligned} |\boldsymbol{\theta}_{\alpha,k}\mathbf{b}_k + h_{d,k}| &\le \sum_{n=1}^{N} |\boldsymbol{\theta}_{\alpha,k}(n)\mathbf{b}_k(n)| + |h_{d,k}| \\ &= \sum_{n=1}^{N} |\mathbf{b}_k(n)| + |h_{d,k}|, \end{aligned} \tag{22}$$

where $\mathbf{b}_k(n)$ denotes the n-th element of $\mathbf{b}_k$; The equality holds in (22) with the unit-modulus constraint $|\boldsymbol{\theta}_{\alpha,k}(n)| = 1,\ \forall k \in [1, K],\ \forall n \in [1, N]$. The optimal solution of $\boldsymbol{\theta}_{\alpha,k}$ can be obtained by solving the upper bound in (22) with respect to $\boldsymbol{\theta}_{\alpha,k}(n)$. On the other hand, this upper bound holds with $\alpha^*_{k,n} = \arg(h_{d,k}) - \arg(\mathbf{b}_k[n])$, where $\arg(\cdot)$ is the phase operator [9], [11]. Accordingly, the optimal solution of $\boldsymbol{\theta}_{\alpha,k}$ is expressed as $\boldsymbol{\theta}^*_{\alpha,k} = \left[\exp\left(j\alpha^*_{k,1}\right), ..., \exp\left(j\alpha^*_{k,N}\right)\right]$. Thus, we completed the proof of *Theorem* 1. ∎

C. Optimal Design of $\boldsymbol{\theta}_{\alpha,0}$

After obtaining the optimal solution of $\boldsymbol{\theta}_{\alpha,k}$, we denote $\tilde{t}_{1,k} = \left|\boldsymbol{\theta}^*_{\alpha,k}\mathbf{b}_k + h_{d,k}\right|^2$, and substitute it into problem (19), then we have,

$$\begin{aligned} &\max_{\boldsymbol{\theta}_{\alpha,0}} \ \sum_{k=1}^{K} \frac{\tilde{A}_k |\boldsymbol{\theta}_{\alpha,0}\mathbf{a}_k + g_{d,k}|^2}{B_k |\boldsymbol{\theta}_{\alpha,0}\mathbf{a}_k + g_{d,k}|^2 + c_k^2}, \\ &\ s.t. \ |\boldsymbol{\theta}_{\alpha,0}(n)| = 1,\ \forall n \in [1, N], \end{aligned} \tag{23}$$

where $\tilde{A}_k = A_k\tilde{t}_{1,k}$. To solve problem (23), we first consider the quadratic transformation (QT) [20] to transform its fractional objective function into the following subtractive form by introducing an auxiliary variable vector $\boldsymbol{\xi} = [\xi_1, ..., \xi_K]^T \in \mathbb{C}^{K\times 1}$ as below

$$\begin{aligned} &\sum_{k=1}^{K} 2\sqrt{\tilde{A}_k}\Re\left\{\mathrm{conj}(\xi_k)\boldsymbol{\theta}_{\alpha,0}\mathbf{a}_k + \mathrm{conj}(\xi_k)g_{d,k}\right\} \\ &\qquad - \sum_{k=1}^{K} |\xi_k|^2 \left(B_k |\boldsymbol{\theta}_{\alpha,0}\mathbf{a}_k + g_{d,k}|^2 + c_k^2\right), \end{aligned} \tag{24}$$

where

$$\xi_k^* = \frac{\sqrt{\tilde{A}_k}\left(\boldsymbol{\theta}_{\alpha,0}\mathbf{a}_k + g_{d,k}\right)}{B_k |\boldsymbol{\theta}_{\alpha,0}\mathbf{a}_k + g_{d,k}|^2 + c_k^2}. \tag{25}$$

Next, we alternately optimize the variables $\boldsymbol{\theta}_{\alpha,0}$ and $\boldsymbol{\xi}$. Specifically, we optimally design $\boldsymbol{\theta}_{\alpha,0}$ for given $\boldsymbol{\xi}$, which is then optimized by (25) at each iteration. For the fixed $\boldsymbol{\xi}$, problem (23) can be transformed as

$$\begin{aligned} &\max_{\boldsymbol{\theta}_{\alpha,0}} \ \sum_{k=1}^{K} 2\sqrt{\tilde{A}_k}\Re\left\{\mathrm{conj}(\xi_k)\boldsymbol{\theta}_{\alpha,0}\mathbf{a}_k + \mathrm{conj}(\xi_k)g_{d,k}\right\} \\ &\qquad - \sum_{k=1}^{K} |\xi_k|^2 \left(B_k |\boldsymbol{\theta}_{\alpha,0}\mathbf{a}_k + g_{d,k}|^2 + c_k^2\right), \\ &\ s.t. \ |\boldsymbol{\theta}_{\alpha,0}(n)| = 1,\ \forall n \in [1, N]. \end{aligned} \tag{26}$$

To make problem (26) more tractable, we proceed to manipulate its objective function as

$$\begin{aligned} &\sum_{k=1}^{K} 2\sqrt{\tilde{A}_k}\Re\left\{\mathrm{conj}(\xi_k)\boldsymbol{\theta}_{\alpha,0}\mathbf{a}_k + \mathrm{conj}(\xi_k)g_{d,k}\right\} \\ &\qquad - \sum_{k=1}^{K} |\xi_k|^2 \left(B_k |\boldsymbol{\theta}_{\alpha,0}\mathbf{a}_k + g_{d,k}|^2 + c_k^2\right), \\ &= -\boldsymbol{\theta}_{\alpha,0}\boldsymbol{\Phi}_0\boldsymbol{\theta}_{\alpha,0}^H + 2\Re\left\{\boldsymbol{\theta}_{\alpha,0}\left(\boldsymbol{\gamma}_1 - \boldsymbol{\gamma}_0\right)\right\} + (d_1 - d_0) \triangleq f_1(\boldsymbol{\theta}_{\alpha,0}), \end{aligned} \tag{27}$$

where

$$\begin{aligned} &\boldsymbol{\Phi}_0 = \sum_{k=1}^{K} |\xi_k|^2 B_k\mathbf{a}_k\mathbf{a}_k^H,\ \boldsymbol{\gamma}_0 = \sum_{k=1}^{K} |\xi_k|^2 B_k\mathrm{conj}\left(g_{d,k}\right)\mathbf{a}_k, \\ &\boldsymbol{\gamma}_1 = \sum_{k=1}^{K} \sqrt{\tilde{A}_k}\mathrm{conj}\left(\xi_k\right)\mathbf{a}_k, \\ &d_0 = \sum_{k=1}^{K} |\xi_k|^2 B_k g_{d,k}\mathrm{conj}\left(g_{d,k}\right) + \sum_{k=1}^{K} |\xi_k|^2 c_k^2, \\ &d_1 = 2\Re\left\{\sum_{k=1}^{K} \sqrt{\tilde{A}_k}\mathrm{conj}\left(\xi_k\right)g_{d,k}\right\}. \end{aligned}$$

Without loss of generality and for convenience, we omit the constant term $d_1 - d_0$, then problem (26) can be equivalently reformulated as

$$\begin{aligned} &\min_{\boldsymbol{\theta}_{\alpha,0}} \ \boldsymbol{\theta}_{\alpha,0}\boldsymbol{\Phi}_0\boldsymbol{\theta}_{\alpha,0}^H - 2\Re\left\{\boldsymbol{\theta}_{\alpha,0}\boldsymbol{\gamma}\right\}, \\ &\ s.t. \ |\boldsymbol{\theta}_{\alpha,0}(n)| = 1,\ \forall n \in [1, N], \end{aligned} \tag{28}$$

where $\boldsymbol{\gamma} = \boldsymbol{\gamma}_1 - \boldsymbol{\gamma}_0$. To solve (28), we propose to utilize the CCM algorithm to iteratively derive the optimal IRS phase shifts $\boldsymbol{\theta}_{\alpha,0}$. The main idea is to focus on the derivation of a gradient descent algorithm over the manifold space [21]. To perform this method, problem (28) is first reformulated as

$$\begin{aligned} &\min_{\boldsymbol{\theta}_{\alpha,0}} \ f_3(\boldsymbol{\theta}_{\alpha,0}) = \boldsymbol{\theta}_{\alpha,0}\left(\boldsymbol{\Phi}_0 + \kappa\mathbf{I}_N\right)\boldsymbol{\theta}_{\alpha,0}^H - 2\mathcal{R}\left\{\boldsymbol{\theta}_{\alpha,0}\boldsymbol{\gamma}_0\right\}, \\ &\ s.t. \ |\boldsymbol{\theta}_{\alpha,0}(n)| = 1,\ \forall n \in [1, N], \end{aligned} \tag{29}$$

where $\kappa > 0$ is used to control the convergence of the CCM algorithm. Also, problem (28) is equivalent to (29) due to $\kappa\boldsymbol{\theta}_{\alpha,0}\boldsymbol{\theta}_{\alpha,0}^H = \kappa N$. The feasible set of problem (29) is considered as the product of N complex circles, i.e., $\mathcal{S}^N$, each of which is one complex circle defined as $\mathcal{S} \triangleq \left\{z \in \mathbb{C} : \mathrm{conj}(z)z = \Re\{z\}^2 + \Im\{z\}^2 = 1\right\}$. The set $\mathcal{S}$ can be regarded as a sub-manifold of $\mathbb{C}$, and the product of N circles is accordingly a sub-manifold of $\mathbb{C}^N$ [21]. Thus, the manifold of (29) is given as $\mathcal{S}^N \triangleq \left\{\mathbf{z} \in \mathbb{C}^N : |\mathbf{z}(n)| = 1, n \in [1, N]\right\}$, where $\mathbf{z}(n)$ is the n-th element of vector $\mathbf{z}$. To proceed, we characterize the main procedures of the CCM algorithm to iteratively solve problem (29), which includes the following steps at each iteration.

1) We first search the direction to minimize problem (29), which is opposite to the gradient in Euclidean space of $f_3(\boldsymbol{\theta}_{\alpha,0}^{(i)})$, i.e.,

$$\boldsymbol{\iota}^{(i)}=-\nabla_{\boldsymbol{\theta}_{\alpha,0}} f_3(\boldsymbol{\theta}_{\alpha,0}^{(i)})=-2\left(\boldsymbol{\Phi}_0+\kappa\mathbf{I}_N\right)\left(\boldsymbol{\theta}_{\alpha,0}^{(i)}\right)^H+2\boldsymbol{\gamma}_0. \tag{30}$$

2) The optimization step is performed to find the *Riemannian gradient* of $f_3(\boldsymbol{\theta}_{\alpha,0}^{(i)})$ at $\boldsymbol{\theta}_{\alpha,0}^{(i)} \in \mathcal{S}^N$ based on the tangent space $\mathcal{T}_{\boldsymbol{\theta}_{\alpha,0}^{(m)}}\mathcal{S}^N$ [22]. To proceed, we project the search direction $\boldsymbol{\iota}^{(i)}$ in Euclidean space onto $\mathcal{T}_{\boldsymbol{\theta}_{\alpha,0}^{(i)}}\mathcal{S}^N$, and the *Riemannian* gradient of $f_3(\boldsymbol{\theta}_{\alpha,0}^{(i)})$ at $\boldsymbol{\theta}_{\alpha,0}^{(i)}$ is given as follows [22]:

$$\mathbf{P}_{\mathcal{T}_{\boldsymbol{\theta}_{\alpha,0}^{(i)}}\mathcal{S}^N}(\boldsymbol{\iota}^{(i)})=\boldsymbol{\iota}^{(i)}-\Re\left\{\mathrm{conj}(\boldsymbol{\iota}^{(i)})\odot\boldsymbol{\theta}_{\alpha,0}^{(i)}\right\}\odot\boldsymbol{\theta}_{\alpha,0}^{(i)}. \tag{31}$$

3) We proceed to update $\boldsymbol{\theta}_{\alpha,0}^{(i)}$ on the tangent space $\mathcal{T}_{\boldsymbol{\theta}_{\alpha,0}^{(i)}}\mathcal{S}^N$, which is expressed as

$$\bar{\boldsymbol{\theta}}_{\alpha,0}^{(i)}=\boldsymbol{\theta}_{\alpha,0}^{(i)}+\zeta\mathbf{P}_{\mathcal{T}_{\boldsymbol{\theta}_{\alpha,0}}\mathcal{S}^N}(\boldsymbol{\iota}^{(i)}), \tag{32}$$

where ζ is a step size that will be characterized later.

4) Then, the retraction operation is required to map $\bar{\boldsymbol{\theta}}_{\alpha,0}^{(i)}$ into the manifold $\mathcal{S}^N$, which aims to normalize each element of $\bar{\boldsymbol{\theta}}_{\alpha,0}^{(i)}$ to be unit as follows

$$\boldsymbol{\theta}_{\alpha,0}^{(i+1)}=\bar{\boldsymbol{\theta}}_{\alpha,0}^{(i)}\odot\frac{1}{\bar{\boldsymbol{\theta}}_{\alpha,0}^{(i)}}. \tag{33}$$

Additionally, we consider the following *proposition* to determine the range of κ and ζ.

Proposition 1: [21], [23] The parameters κ and ζ are selected to guarantee $\kappa \geq \frac{N}{8}\varrho_{\max}(\boldsymbol{\Phi}_0)+\|\boldsymbol{\gamma}\|_2$, and $0<\zeta<\frac{1}{\varrho_{\max}(\boldsymbol{\Phi}_0+\kappa\mathbf{I}_N)}$, respectively, which ensures that the CCM algorithm has a non-increasing behaviour until convergence. From the above-mentioned discussion, the detailed steps of the CCM method can be elaborated in *Algorithm* 1.

Algorithm 1: The CCM algorithm

---

1) **Initialization**: i, ε and $\boldsymbol{\theta}_{\alpha,0}^{(0)}$ denote the iteration index, the algorithm accuracy, and the initialized solution, respectively. **Calculate** the initial objective value $f_3(\boldsymbol{\theta}_{\alpha,0}^{(0)})$.
2) **Repeat**:
   a) **Calculate** the search direction $\boldsymbol{\iota}^{(i)}$ in (30).
   b) **Calculate** the projection of $\boldsymbol{\iota}^{(i)}$, i.e., $\mathbf{P}_{\mathcal{T}_{\boldsymbol{\theta}_{\alpha,0}}\mathcal{S}^N}(\boldsymbol{\iota}^{(i)})$, onto the tangent space according to (31).
   c) **Update** $\bar{\boldsymbol{\theta}}_{\alpha,0}^{(i)}$ over the tangent space via (32).
   d) **Retract** $\boldsymbol{\theta}_{\alpha,0}^{(i+1)}$ to the manifold $\mathcal{S}^N$ via (33).
   e) **Set** $i = i+1$ until convergence, i.e., $\frac{\left|f_3(\boldsymbol{\theta}_{\alpha,0}^{(i+1)})-f_3(\boldsymbol{\theta}_{\alpha,0}^{(i)})\right|}{f_3(\boldsymbol{\theta}_{\alpha,0}^{(i+1)})} \leq \varepsilon$.
3) **Obtain** $\boldsymbol{\theta}_{\alpha,0}^{*}$.

The optimal IRS phase shifts $\boldsymbol{\theta}_{\alpha,0}^{(i+1)}$ can be computed in Step 2-d) of *Algorithm* 1, thus, *Algorithm* 1 can guarantee that the objective value $f_3(\boldsymbol{\theta}_{\alpha,0}^{(i+1)})$ has a monotonically non-increasing behaviour. The solution $\boldsymbol{\theta}_{\alpha,0}^{(i+1)}$ is updated by *Algorithm* 1 at the $(i+1)$-th iteration to satisfy $f_3(\boldsymbol{\theta}_{\alpha,0}^{(i)}) > f_3(\boldsymbol{\theta}_{\alpha,0}^{(i+1)})$. Due to the unit modulus constraint, *Algorithm* 1 can achieve the convergence.

From the aforementioned analysis, we clarify the overall steps of the proposed scheme in *Algorithm* 2.

Algorithm 2: The proposed algorithm to solve problem (4)

---

1) **Obtain** the optimal solution of $\boldsymbol{\theta}_{\alpha,k},\ \forall k \in [1,K]$ by *Theorem* 1.
2) **Initialization**: let $\boldsymbol{\xi}^{(0)}$ be a feasible vector, and the number of iteration be $l=1$.
3) **Repeat**
   a) **Solve** problem (23) to update $\boldsymbol{\theta}_{\alpha,0}^{(l)}$ by the CCM algorithm in *Algorithm* 1.
   b) **Update** $\boldsymbol{\xi}^{(l)}=\left[\xi_1^{(l)},...,\xi_K^{(l)}\right]^T$, where $\xi_k^{(l)}=\xi_k^*$ can be obtained by (25).
   c) **Set** $l=l+1$ until the algorithm converges.
   d) **Obtain** the locally optimal solution $\boldsymbol{\theta}_{\alpha,0}^{*}$ and $\boldsymbol{\xi}^*$.
4) **Substitute** $\boldsymbol{\theta}_{\alpha,k}^{*},\ \forall k \in [0,K]$ into (18) to calculate τ_0^*.
5) **Substitute** τ_0^* into (14) to calculate $\tau_k^*,\ \forall k \in [1,K]$.

Now, we characterize the convergence of *Algorithm* 2. This algorithm consists of an alternating procedure of CCM and QT method to design the IRS phase shifts $\boldsymbol{\theta}_{\alpha,0}$ by iteratively solving the sum of fractional programmings in (26). It is readily verified that (26) is a convex optimization problem due to the concave-convex form of (23) [20]. Also, the first-order condition on $\boldsymbol{\theta}_{\alpha,0}$ for (26) for given $\boldsymbol{\xi}^*$ is identical to problem (23) due to the equivalent conditions in solution and objective value [20, C2,C3]. Via every update of $\boldsymbol{\xi}$, the objective value of the sum of fractional programming values in (23) provides a non-decreasing behaviour and converges to a stationary point $(\boldsymbol{\theta}_{\alpha,0}^{*},\boldsymbol{\xi}^*)$ of (26). In addition, we numerically validate the convergence of *Algorithm* 2 in Section IV.

IV. Numerical Results

This section demonstrates numerical results to evaluate the considered system, where its deployment is depicted in Fig. 3 in terms of a three-dimensional (3-D) coordinate. As it can be seen, PS, AP, and IRS are deployed at $(X_{PS},Y_{PS},Z_{PS})=(-10,0,0)$, $(X_{AP},Y_{AP},Z_{AP})=(10,0,0)$ and $(X_{IRS},Y_{IRS},Z_{IRS})=(-2,6,0)$, respectively. The k-th IoT device, i.e., $\mathcal{U}_k,\ \forall k \in [1,K]$, is deployed at (X_k,Y_k,Z_k), which is randomly distributed within a circular area of $x-z$ coordinate centered $(0,0)$ and radius 5 m. The channel coefficients of the IRS related links, i.e., $\mathbf{g}_0$, $\mathbf{g}_{r,k}$, $\mathbf{h}_k$, $\mathbf{h}_r$, are modelled as Rician fading, and the channel coefficients of the direct links, i.e., $\mathbf{g}_{d,k}$ and $\mathbf{h}_{d,k}$, are modelled as Rayleigh fading [11]. In addition, we set the path loss model to $P_L=Ad_q^{\epsilon_q}$, where $A=-30$ dBm, d_q

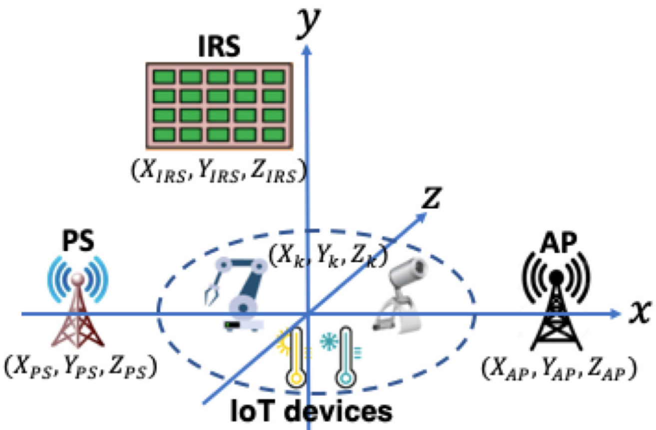

Fig. 3: System deployment.

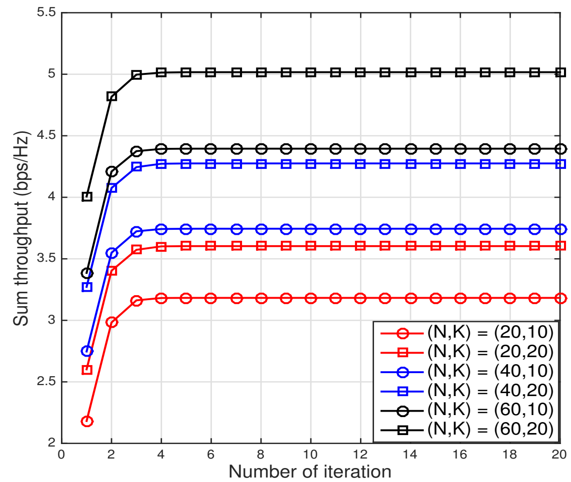

Fig. 4: Convergence of *Algorithm* 2.

and ϵ_q, $\forall q \in \{PS2IRS, IRS2U, IRS2AP, PS2U, U2AP\}$, represent the physical distance and the path loss exponent between the PS and the IRS, the IRS and $\mathcal{U}_k$, the IRS and the AP, the PS and $\mathcal{U}_k$, as well as $\mathcal{U}_k$ and the AP, respectively. Unless otherwise specified, other simulation parameters are summarized in Table I on the top of the next page.

To highlight the proposed scheme, we consider the following benchmark schemes for comparison with the same setup:

1) *Linear energy harvesting (LEH) model*: The IRS's phase shifts and transmission time scheduling are jointly optimized based on the LEH model [9].
2) *Random phase shifts*: Each phase shift is randomly generated at $[0, 2\pi]$ with the optimal design of the transmission time scheduling.
3) *Equal transmission time scheduling*: The IRS's phase shifts are optimally designed with equal transmission time allocation.
4) *Discrete phase shifts*: Each phase shift is selected from a finite number of phase shifts, and its discrete phase shift set is expressed as $\mathcal{S}_d = \left\{0, \frac{2\pi}{2^{B_0}}, \dots, \frac{(2^{B_0}-1)2\pi}{2^{B_0}}\right\}$, where B_0 represents the bit number used to indicate the number of phase resolutions.
5) *Without IRS*: The system model is degraded to a traditional wireless powered IoT network [5].

First, Fig. 4 shows how *Algorithm* 2 converges with different numbers of IRS reflecting elements N and IoT devices K, where the sum throughput exhibits an monotonically increasing trend and then reaches its convergence approximately at the fourth or fifth iteration. This validates the proposed QT and CCM methods for iteratively designing the IRS phase shifts.

Next, the impact of the transmit power P_0 on the sum throughput is shown in Fig. 5, where all schemes provides a monotonically increasing trend with respect to P_0. Also, the proposed NLEH model outperforms the other benchmark schemes, i.e., equal time allocation, random phase shifts, and without IRS, which is explained by emphasising the optimal designs of the IRS phase shifts and the time durations. Additionally, it is expected to show that the LEH model provides an upper bound on the sum throughput of the proposed NLEH model, this is because the energy conversion efficiency η of the LEH model leads to an ideal case which outperforms the NLEH model. Fig. 6 illustrates the sum throughput per-

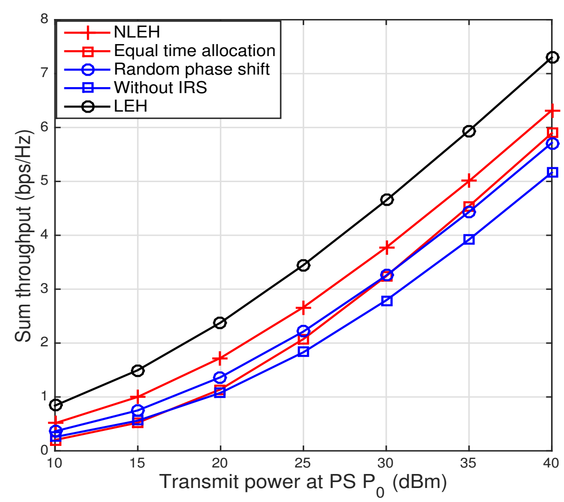

Fig. 5: Sum throughput versus transmit power at PS P_0.

formance with respect to the number of the IRS reflecting elements N. For the IRS related schemes, i.e., NLEH, LEH, equal time allocation, and random phase shifts, the sum throughput shows a monotonically increasing behaviour with N, whereas for the scheme without IRS it remains constant with N. The proposed NLEH scheme outperforms that of the equal time allocation, the random phase shifts, and without IRS, which highlights the benefits induced by the IRS and verifies the optimization of the transmission time scheduling. Additionally, the LEH model outperforms the NLEH model by a significant margin. Fig. 7 evaluates the impact of different numbers of IoT devices K on the sum throughput. The sum throughput demonstrates a monotonically increasing behaviour as K increases, and the proposed NLEH scheme demonstrates a better performance in comparison to that with discrete phase shifts, with equal transmission allocation, and without IRS,

TABLE I: **Simulation Parameters**

Parameters	Values	Parameters	Values
Transmit power at the PS	$P_0 = 30$ dBm or 1 W	Number of IoT devices	$K = 5$, 10, or 20
Number of reflecting elements	$N = 50$	Whole time duration	$T = 1$ second
Available bandwidth	1 MHz	Noise power density	-170 dBm/Hz
Energy conversion efficiency	$\eta = 0.8$	Path loss exponents	$\epsilon_{PS2IRS} = \epsilon_{IRS2AP} = 2$
Amplitude of reflection coefficient	$\beta_{k,n} = 1,\ \forall k \in [0, K],\ \forall n \in [1, N]$		$\epsilon_{IRS2U} = 2.5$, $\epsilon_{PS2U} = \epsilon_{U2AP} = 3.5$

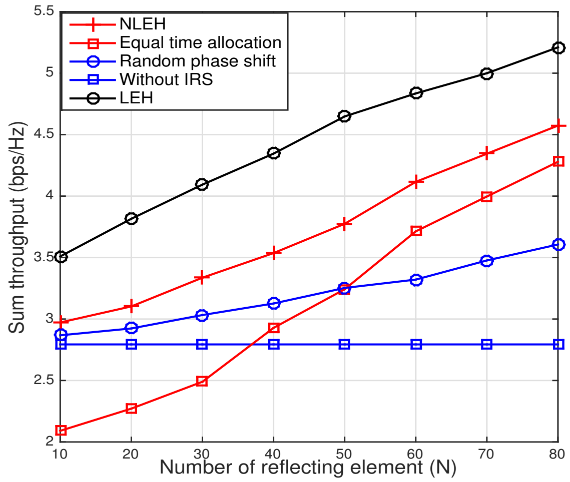

Fig. 6: Sum throughput versus number of IRS reflecting elements N.

which confirms the optimality of IRS phase shifts design, and the benefits induced by the IRS.

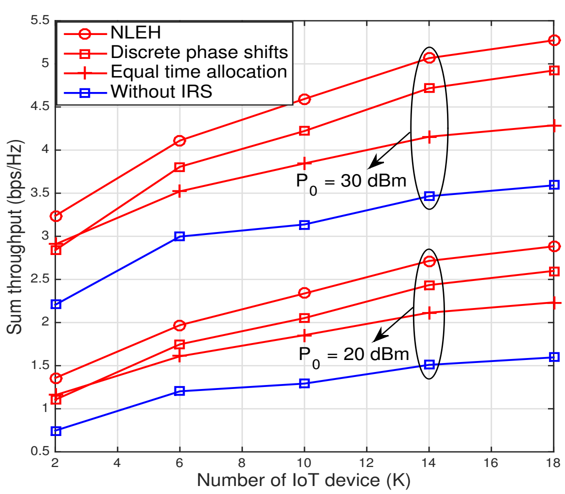

Fig. 7: Sum throughput versus number of IoT devices K.

Then, Fig. 8 demonstrates the impact of x-coordinate of the IRS X_{IRS} on the sum throughput. From this figure, the sum throughput of the IRS assisted schemes first has an increasing trend and then declines with respect to X_{IRS} compared with that without IRS, which remains constant with X_{IRS}. This highlights the optimal IRS deployment to achieve the best performance gain. In addition, the proposed NLEH scheme outperforms the cases with equal time allocation, random phase shifts, and no IRS, which exhibits the optimal designs of the time scheduling and IRS phase shifts, plus the benefits induced by the IRS. In Fig. 9, we evaluate the impact of

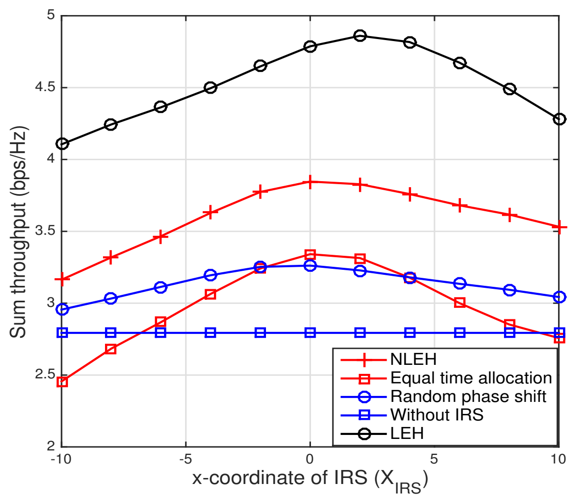

Fig. 8: Sum throughput versus x-coordinate of IRS X_{IRS}.

the path loss exponents of the IRS related links, i.e., PS-IRS (ϵ_{PR2IRS}), IRS-$\mathcal{U}_k$ (ϵ_{IRS2U}), as well as IRS-AP (ϵ_{IRS2AP}). For the proposed scheme, the sum throughput declines with respect to ϵ_{PR2IRS}, ϵ_{IRS2U}, or ϵ_{IRS2AP}, outperforming that without IRS which remains constant with these three path loss exponents. This releases a fact that larger-scale fading gives rise to a weaker energy/information reflection induced by the IRS, and in turn diminishes its beneficial role at the duration of WET and WIT.

Moreover, we exhibit the sum throughput with different numbers of bits $B_0 \in [1\text{ bit}, 8\text{ bits}]$ to characterize the discrete phase resolution of the IRS in Fig. 10. As shown in this figure, the case with continuous phase shifts remains constant and provides an upper bound on its discrete counterpart, and the performance gap between them gradually diminishes as B_0 increases. This could be due to the quantized IRS phase resolutions causing an imperfect alignment, which degrades system performance during the WET and WIT phases. Also, a higher interval density of the discrete phase resolutions would allow for more efficient energy/information reflection, with sum throughput approaching that of the continuous counterpart.

Furthermore, we present the optimal energy time duration τ_0 and the sum harvested energy versus N in Fig. 11 and Fig. 12, respectively. In Fig. 11, the optimal energy time τ_0 shows a monotonically decreasing behaviour with respect to N for the LEH and NLEH models, which consume less time for

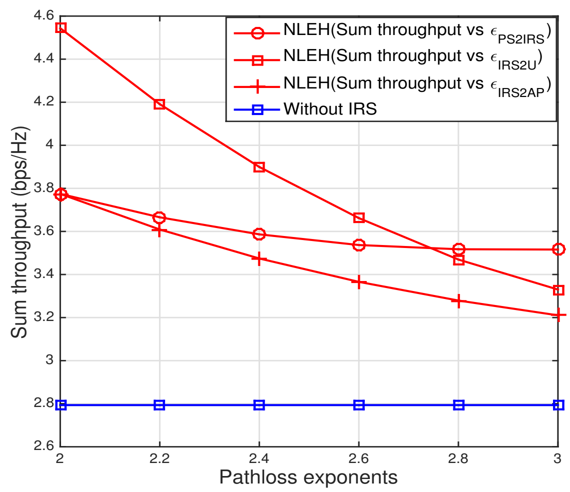

Fig. 9: Sum throughput versus path-loss exponents.

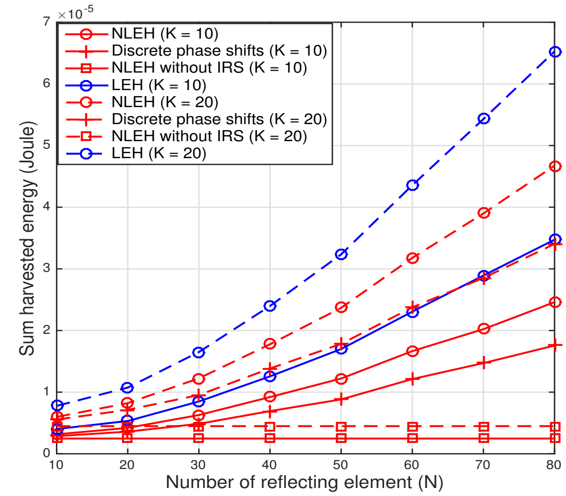

Fig. 12: Sum harvested energy versus number of IRS reflecting elements N.

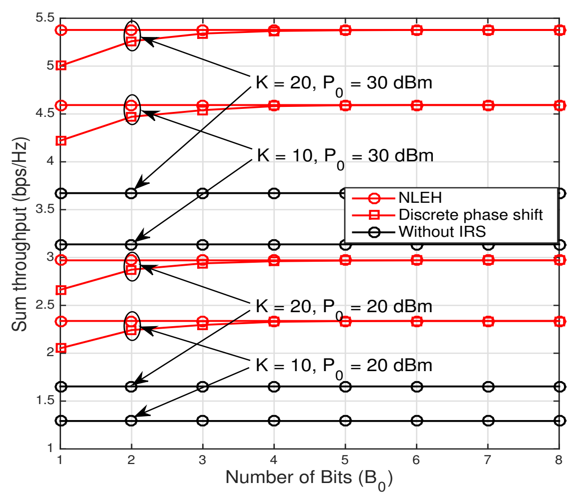

Fig. 10: Sum throughput versus number of bits B_0.

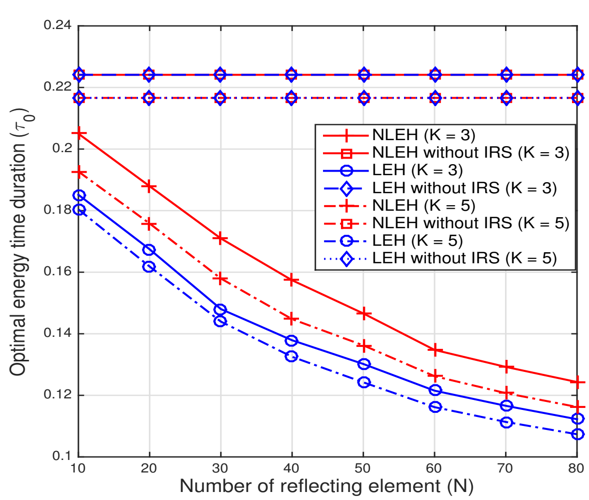

Fig. 11: Optimal energy time slot τ_0 versus number of IRS reflecting elements N.

downlink WET than that without IRS. This further implies an energy saving at the PS, which is beneficial and leaves more time duration for the IoT devices for uplink WIT to enhance the throughput performance. In addition, larger number of IoT devices K can consume less time for downlink WET, which can be explained by the fact that more time slots may be consumed due to larger K to guarantee the throughput performance of uplink WIT. Fig. 12 demonstrates that the sum harvested energy of all IoT devices monotonically increases in terms of N, which reveals a fact that the decline of τ_0 may not at a cost of the harvested energy for the IoT devices. This is due to the fact that the energy reflection at the IoT devices can be effectively improved with the aid of IRS in comparison to that with the discrete phase shifts, and without IRS, which validates the optimal design of the IRS phase shifts and the IRS's beneficial role in terms of energy harvesting capability. As such, the utilization of IRS in the wireless powered network can not only provide a throughput improvement at the AP but also guarantee energy saving at the PS, enjoying a spectral and energy-efficient framework.

Finally, we examine the sum throughput versus N for larger numbers of IoT devices, i.e., $K = 10$ or 20, and make a comparison between the proposed NLEH model and the Sigmoid function based NLEH model [14]. Aside the similar increasing behaviour of the sum throughput to Fig. 6, one can observe that a larger number of IoT devices can play a positive role in improving the network throughput performance. Also, the proposed NLEH model significantly outperforms the existing Sigmoid function based NLEH model, which confirms the advantage of the proposed scheme.

V. Conclusion

This paper revealed the NLEH's potential in the wireless powered intelligent radio environment. The sum throughput maximization problem of the considered system was formulated and solved to characterize its overall performance by jointly designing the IRS phase shifts as well as the transmis-

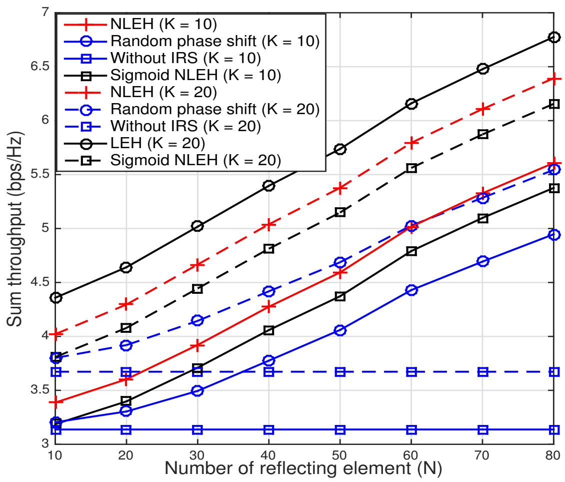

Fig. 13: Sum throughput versus number of IRS reflecting elements N with different numbers of IoT devices and comparison between the proposed scheme and the Sigmoid function based NLEH model.

sion time scheduling. To address the formulated problem, the Lagrange dual method and KKT conditions were proposed to optimally derive the closed form solution of the transmission time scheduling. Also, we proposed the QT to transform the summation of multiple fractional programmings to the subtracted form, which was then tackled by the CCM method to iteratively design the optimal solution of the IRS phase shifts. Finally, simulation results was exhibited to highlight the optimal designs of the transmission time scheduling and the IRS phase shifts, as well as the benefits induced by the IRS compared to the benchmark schemes. For our future work, we will consider a novel time allocation scheme, where each IoT device keeps active for harvesting energy while others are busy for transmitting their own information to the AP. This scenario may result in a more complicated problem formulation such that the proposed scheme in this work may not be feasible, necessitating a different approach to deal with it.

REFERENCES

[1] M. D. Renzo, A. Zappone, M. Debbah, M. Alouini, C. Yuen, J. D. Rosny, and S. Tretyakov, “Smart radio environments empowered by reconfigurable intelligent surfaces: How it works, state of research, and road ahead,” *IEEE J. Sel. Areas Commun.*, vol. 38, no. 11, pp. 2450 – 2525, Nov. 2020.

[2] C. Huang, S. Hu, G. C. Alexandropoulos, A. Zappone, C. Yuen, R. Zhang, M. Di Renzo, and M. Debbah, “Holographic MIMO surfaces for 6G wireless networks: Opportunities, challenges, and trends,” *to appear in IEEE Wireless Commun.*, 2020.

[3] Q. Wu and R. Zhang, “Intelligent reflecting surface enhanced wireless network via joint active and passive beamforming,” *IEEE Trans Wireless Commun.*, vol. 18, no. 11, pp. 5394–5409, Nov. 2019.

[4] C. Huang, A. Zappone, G. C. Alexandropoulos, M. Debbah, and C. Yuen, “Reconfigurable intelligent surfaces for energy efficiency in wireless communication,” *IEEE Trans. Wireless Commun.*, vol. 18, no. 8, pp. 4157–4170, Aug. 2019.

[5] H. Ju and R. Zhang, “Throughput maximization in wireless powered communication networks,” *IEEE Trans. Wireless Commun.*, vol. 13, no. 1, pp. 418–428, Jan. 2014.

[6] Q. Wu and R. Zhang, “Weighted sum power maximization for intelligent reflecting surface aided SWIPT,” *IEEE Wireless Commun. Lett.*, vol. 9, no. 5, pp. 586–590, May 2020.

[7] Q. Wu and R. Zhang, “Joint active and passive beamforming optimization for intelligent reflecting surface assisted SWIPT under QoS constraints,” *IEEE J. Sel. Areas Commun.*, vol. 38, no. 8, pp. 1735–1748, Aug. 2020.

[8] C. Pan, H. Ren, K. Wang, M. Elkashlan, A. Nallanathan, J. Wang, and L. Hanzo, “Intelligent reflecting surface aided MIMO broadcasting for simultaneous wireless information and power transfer,” *IEEE J. Sel. Areas Commun.*, vol. 38, no. 8, pp. 1719–1734, Aug. 2020.

[9] Z. Chu, Z. Zhu, F. Zhou, M. Zhang, and N. Al-Dhahir, “Intelligent reflecting surface assisted wireless powered sensor networks for internet of things,” *to appear in IEEE Trans. Commun.*, pp. 1–1, 2021.

[10] B. Lyu, P. Ramezani, D. T. Hoang, S. Gong, Z. Yang, and A. Jamalipour, “Optimized energy and information relaying in self-sustainable IRS-empowered WPCN,” *IEEE Trans. Commun.*, vol. 69, no. 1, pp. 619–633, 2021.

[11] Z. Chu, P. Xiao, D. Mi, W. Hao, M. Khalily, and L.-L. Yang, “A novel transmission policy for intelligent reflecting surface assisted wireless powered sensor networks,” *IEEE Journal of Selected Topics in Signal Processing*, pp. 1–1, 2021.

[12] Q. Wu, X. Zhou, and R. Schober, “IRS-assisted wireless powered NOMA: Do we really need different phase shifts in DL and UL?,” *to appear in IEEE Wireless Commun. Lett.*, pp. 1–1, 2021.

[13] D. Zhang, Q. Wu, M. Cui, G. Zhang, and D. Niyato, “Throughput maximization for IRS-assisted wireless powered hybrid NOMA and TDMA,” *to appear in IEEE Wireless Commun. Lett.*, pp. 1–1, 2021.

[14] D. Xu, X. Yu, V. Jamali, D. W. K. Ng, and R. Schober, “Resource allocation for large IRS-assisted SWIPT systems with non-linear energy harvesting model,” in *IEEE WCNC, Nanjing, China*, pp. 1–7, 2021.

[15] S. Zargari, A. Khalili, Q. Wu, M. Robat Mili, and D. W. K. Ng, “Max-min fair energy-efficient beamforming design for intelligent reflecting surface-aided SWIPT systems with non-linear energy harvesting model,” *to appear in IEEE Trans. Vehicular Technol.*, pp. 1–1, 2021.

[16] S. Zargari, S. Farahmand, B. Abolhassani, and C. Tellambura, “Robust active and passive beamformer design for IRS-aided downlink MISO PS-SWIPT with a nonlinear energy harvesting model,” *to appear in IEEE Trans. Green Commun. Netw.*, pp. 1–1, 2021.

[17] Z. Li, W. Chen, Q. Wu, H. Cao, K. Wang, and J. Li, “Robust beamforming design and time allocation for IRS-assisted wireless powered communication networks,” 2021.

[18] Y. Chen, N. Zhao, and M.-S. Alouini, “Wireless energy harvesting using signals from multiple fading channels,” *IEEE Trans. Commun.*, vol. 65, no. 11, pp. 5027–5039, Nov. 2017.

[19] S. Boyd and L. Vandenberghe, *Convex Optimization*. Cambridge, UK: Cambridge University Press, 2004.

[20] K. Shen and W. Yu, “Fractional programming for communication systems - Part I: Power control and beamforming,” *IEEE Trans. Signal Process.*, vol. 66, no. 10, pp. 2616–2630, May 2018.

[21] K. Alhujaili, V. Monga, and M. Rangaswamy, “Transmit MIMO radar beampattern design via optimization on the complex circle manifold,” *IEEE Trans. Signal Process,*, vol. 67, no. 13, pp. 3561–3575, Jul. 2019.

[22] X. Yu, J. Shen, J. Zhang, and K. B. Letaief, “Alternating minimization algorithms for hybrid precoding in millimeter wave MIMO systems,” *IEEE J. Sel. Topics Signal Process.*, vol. 10, no. 3, pp. 485–500, Apr. 2016.

[23] C. Pan, H. Ren, K. Wang, W. Xu, M. Elkashlan, A. Nallanathan, and L. Hanzo, “Multicell MIMO communications relying on intelligent reflecting surfaces,” *IEEE Trans. Wireless Commun.*, vol. 19, no. 8, pp. 5218–5233, Aug. 2020.